Bollettino di Geofisica Teorica ed Applicata Vol. 62, n. 1, pp. 19-32; March 2021
DOI 10.4430/bgta0341

Temporal variations of *b*-values in central Ionian Islands (Greece)

O. Mangira, E. Papadimitriou and V. Karakostas

Department of Geophysics, School of Geology, Aristotle University of Thessaloniki, Greece

(Received: 22 December 2019; accepted: 27 July 2020)

ABSTRACT Investigation of temporal *b*-values variations during the last decade is attempted in central Ionian Islands (Greece), the most seismically active area in the Mediterranean area. The high quality catalogue used, starting in 2008 with the completeness magnitude M_c 2.8 comprises data from the aftershock sequences of the 2014 Cephalonia doublet (M_w 6.1 and M_w 6.0) and the 2015 Leukas M_w 6.5 mainshock along with periods of relative quiescence. The analysis is performed by means of two alternative techniques, the "fixed - number - of - events" and the "constant - time - windows" approaches. The results indicate that *b*-value variations are inversely proportional to the seismicity rate with the decreases representing high seismic moment release. For a more detailed monitoring of the fluctuation of *b*-values in time and space, the competently elaborated 2015 Leukas sequence is employed. The results indicate that during the sequence, immediately after the occurrence of the mainshock and for about a month, a decrease in *b*-value is observed, which gradually increases towards the background value.

Key words: *b*-value, temporal variation, Ionian Islands, Greece.

1. Introduction

It has been recognised early in the history of seismology that earthquakes cluster in space and time, forming earthquake sequences. They interact through their stress field and can alter the stress state in their surroundings (Stein, 1999), and, consequently, influence the seismicity rate (Ebel *et al*., 2000). These changes can also influence the earthquake frequency magnitude distribution (FMD) of subsequent earthquakes, which is described by the Gutenberg - Richter (GR) law (Gutenberg and Richter, 1944): $\log N = a - bM$, where N is the cumulative number of events with magnitude greater than, or equal to, M, a is a parameter that describes the productivity, i.e. the total number of earthquakes, and b the slope of the FMD. The higher the *b*-value, the smaller the ratio of large versus small magnitudes, and vice versa.

Acoustic emissions during rock fracture experiments in the laboratory indicate that *b*-value is negatively correlated with differential stress (Scholz, 1968, 2015; Amitrano, 2003; Goebel *et al*., 2013). This correlation is also evidenced from natural seismicity (Wiemer and Wyss, 2002; Tormann *et al*., 2014). It is assumed that *b*-value is a kind of "stress-meter" allowing to track and image asperities; future mainshocks are likely to occur in highly stressed areas where low *b*-values are reported (Wiemer and Wyss, 1997, 2002; Schorlemmer *et al*., 2004; Schorlemmer and Wiemer, 2005). The influence of faulting style in the *b*-value has also been explored suggesting

that areas where normal faulting dominates are characterised by the highest *b*-values, the strike-slip faulting regimes by intermediate values, and the thrust faulting areas by the smallest *b*-values (Schorlemmer *et al*., 2005; Gulia and Wiemer, 2010). Petruccelli *et al*. (2018) analysed the relation between *b*-value and style of faulting using slightly different procedures by expressing the *b*-value fluctuations as a function of rake. They found an oscillating behaviour of *b*-value with maxima close to normal mechanisms and minima close to pure inverse mechanisms. The dependencies of *b*-values on both faulting style and depth have been examined by Petruccelli *et al*. (2019), who suggested that faulting style affects the *b*-value more than depth, but the best model performance is achieved when simultaneous dependencies on faulting style and depth are taken into account.

The numerous studies concerning *b*-values are often related to the accuracy of its computation and uncertainties (e.g. Zuniga and Wyss, 1995; Utsu, 1999) or focus on the spatial variations of *b* (Wyss and Wiemer, 2000; Wyss *et al*., 2001; Tormann *et al*., 2014, 2015). Wiemer and Wyss (1997, 2002) correlate highly stress asperities with anomalously low *b*-values along the San Andreas Fault. Tormann *et al*. (2014), based on high resolution *b*-value imaging along faults in California, suggest that the strong variation of *b*-value through space highlights areas of higher likelihood for future rupture initiation and that this variability should be used for hazard analysis instead of assuming bulk *b*-values.

Temporal variations of *b* have also been investigated in relation to earthquake prediction. Cao and Gao (2002) analysed earthquakes beneath the north-eastern Japan Island arc and found that changes in *b*-values are related to increase in seismic moment release and volcanic activity. Gulia *et al*. (2016) incorporate *b*-value changes into short-term risk models by translating time-dependent *b*-values into daily mainshock probabilities in the case of the L'Aquila 2009 sequence. The effect of a mainshock on the size distribution of aftershocks in 58 aftershock sequences in California, Italy, Japan, and Alaska showed that, immediately after an earthquake, the *b*-value increases by 20 - 30%, decreasing the chance of subsequent larger events (Gulia *et al*., 2018). More recently, Gulia and Wiemer (2019) suggested that the temporal variation of the *b*-values can act as a first-order discriminator between aftershocks and precursory seismicity.

The temporal and spatial *b*-value variations are related to limited space and time windows whereas a constant in time *b*-value holds for wide areas (Kagan *et al*., 2010). Although significant variations in *b*-value have been testified in laboratory experiments (e.g. Amitrano, 2003; Schorlemmer *et al*., 2005; Scholz, 2015), when dealing with real earthquake catalogues recent studies suggest that the estimation of *b*-value and its variation is subject to many uncertainties and should be examined with great caution. That is because biases linked to the analysis of the earthquake catalogues can severely affect the *b*-value estimation. Among them, a critical issue concerns the assessment of the magnitude of completeness (Woessner and Wiemer, 2005; Mignan and Woessner, 2012). The limited amount of data in real catalogues, the binning of magnitudes, the assumption that the data are consistent with the GR law and magnitude errors are sources of bias in the estimation of *b*-value deeply investigated by Marzocchi *et al*. (2020).

We focus on investigating the temporal variations of *b*-values in central Ionian Islands (Greece) during the last decade to identify possible relations with the seismicity behaviour. This data-rich case study including the January - February 2014 sequence from the doublet of Cephalonia Island (Karakostas *et al*., 2015) and the 2015 sequence of Leukas Island (Papadimitriou *et al*., 2017) is appealing to seek for correlations between *b*-value changes and fluctuations in the rate of the observed seismicity.

2. Study area and data

The central Ionian Islands area includes Cephalonia and Leukas islands and has been recognised as the most active seismic source in the Aegean and surrounding area (Fig. 1) characterised by noticeable seismic moment rate [~10^{25} dyne×cm×year^{-1}: Papazachos *et al*. (1997)]. It constitutes an active boundary linking the continental collision in the north, that takes place between the Adriatic microplate and the Eurasian plate, and the subduction of the eastern Mediterranean oceanic lithosphere under the Aegean microplate to the south. The dominant regional tectonic feature is the Cephalonia Transform Fault Zone (KTFZ), a dextral strike slip fault zone (Scordilis *et al*., 1985), comprising the Cephalonia and Leukas fault branches with specific fault segments associated with frequent strong (M≥6.0) events.

The most recent main shock (M_w 6.5) occurred on 17 November 2015 onto a fault segment, in the southern part of the Leukas fault branch of KTFZ (Papadimitriou *et al*., 2017). Its magnitude is the largest magnitude ever reported for the Leukas fault branch in the instrumental era and equal to the first main shock of the 1948 doublet (consisting of an M_w 6.5 and an M_w 6.4 mainshocks) that are associated with two adjacent fault segments (Papazachos and Papazachou, 2003). The northern part of the Cephalonia fault branch accommodated a doublet (M_w 6.1 and M_w 6.0) in 2014. The 2014 activity started on 26 January with the first mainshock and its aftershock activity extending over 35 km, much longer than expected from the causative fault segment. The second mainshock occurred seven days later, 3 February, on an adjacent fault segment, most probably triggered by stress transfer due to the first mainshock (Karakostas *et al*., 2015).

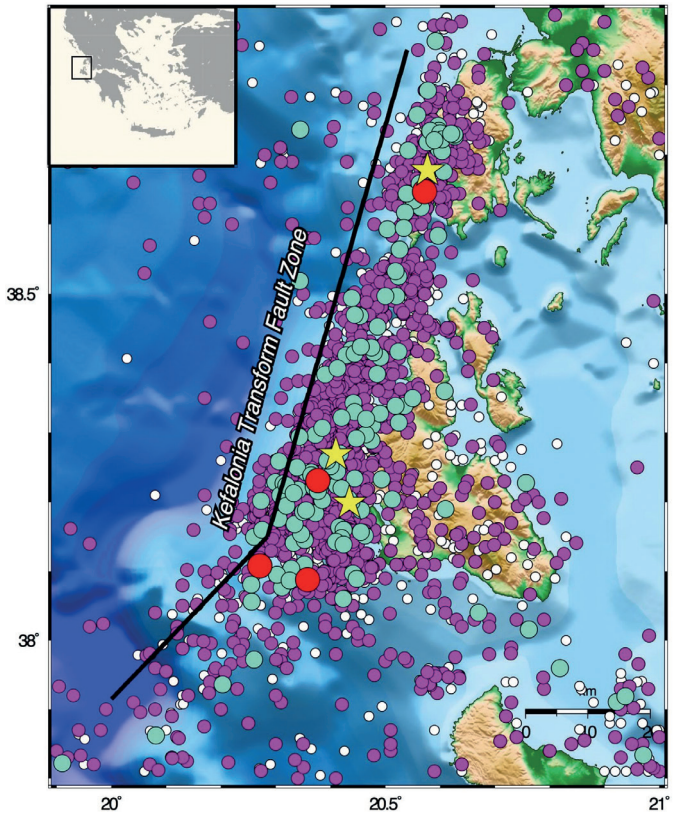

Fig. 1 - Spatial distribution of earthquakes with $M \geq 2.8$ that occurred from January 2008 to December 2017. Events with $2.8 \leq M < 3.0$, $3.0 \leq M < 4.0$, $4.0 \leq M < 5.0$, $5.0 \leq M < 6.0$ are depicted with white, magenta, light blue, and red circles, respectively. Events with $M \geq 6.0$ are depicted with yellow stars.

The use of high quality earthquake catalogues is substantial for the robust estimation of the *b*-values and reliable evaluation of its temporal variations. Particular attention should be paid to the selection of the data in order to avoid artificial changes due to improvements such as recalibrating a magnitude scale, changing the seismological network detectability, or precise relocation feasibility (Zuniga and Wiemer, 1999; Tormann *et al*., 2010; Zuniga *et al*., 2017). The data used in the current study are taken from the catalogue compiled by the Geophysics Department of the Aristotle University of Thessaloniki (Aristotle University of Thessaloniki Seismological Network, 1981) based on the recordings of the Hellenic Unified Seismological Network (HUSN). It is crucial, before estimating the *b*-value changes and trying to recognise patterns and interpret them, to identify M_c. A relatively high magnitude threshold would lead to under-sampling and the discarding of necessary data, whereas a low value would result in a biased analysis, because the data become incomplete (Naylor *et al*., 2010; Mignan and Woesner, 2012).

Before starting the estimations, thorough investigation for the definition of M_c through time is performed. The approach used in our work for examining the time dependence of M_c, is the goodness-of-fit method (GFT; Wiemer and Wyss, 2000). This method computes the difference between the observed FMD and a synthetic one based on the GR law. M_c is found at the first magnitude cutoff M_{co} at which the observed data for $M \geq M_{co}$ is modelled by a straight line for a fixed confidence level, usually 95%. In order to check M_c variability, earthquakes that occurred in the study area since 1980 were considered. The computations are performed in successive sliding windows lasting 1 year and with a step of 1 month. When the coverage and operation of the seismic network is modified, then temporal variations in the M_c are observed (Zuniga *et al*., 2017), which may also arise from the gradual upgrading of the seismic network or due to intense seismic sequences or swarm activity. The increase of the number of seismological stations and updating of the existing hardware and software lead to the improvement of the catalogue completeness and precision over time (Hutton *et al*., 2010; Mignan and Woesner, 2012). We may see in Fig.

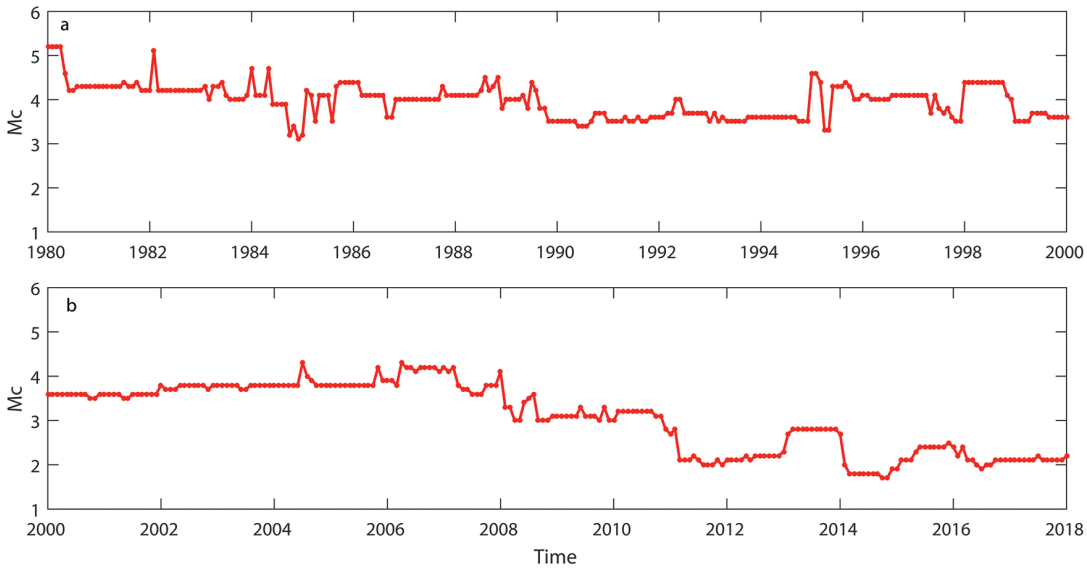

Fig. 2 - Temporal evolution of the minimum magnitude of complete reporting (M_c) using sliding windows of 1 year with step Δt = 1 month: a) time interval 1980 to 2000; b) time interval 2000 to 2017.

2 that as time goes by M_c gets lower. The maximum M_c, equal to 5.2, is found at the beginning of the computations in 1980. The minimum M_c value is computed for the catalogue covering the period between July 2014 and June 2015, i.e. in the time interval between the two sequences. The fluctuation in M_c started to diminish after 2000, when it decreases and is bounded to values below 3.7 almost in all 1-year time windows, whereas after 2008, M_c attains values lower than 3.0.

The decrease of the M_c value is also evidenced by the temporal distribution of earthquake magnitudes since 1980 (Fig. 3). It is clearly shown that a remarkable change takes place after 2007, since when the network detectability was improved and smaller magnitude earthquakes are recorded. Thus, the temporal variations of *b*-values started to be computed since 2008 (Fig. 4).

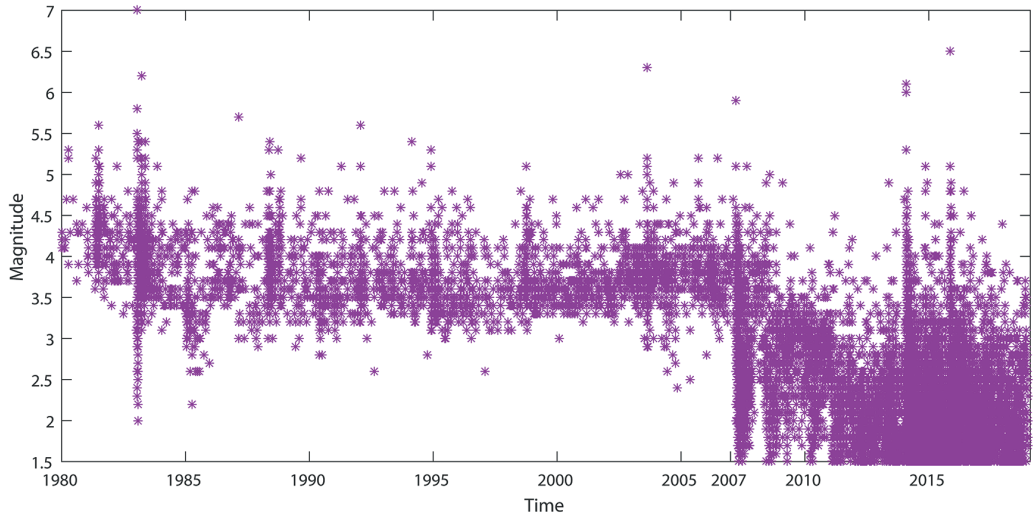

Fig. 3 - Temporal distribution of earthquakes recorded since 1980.

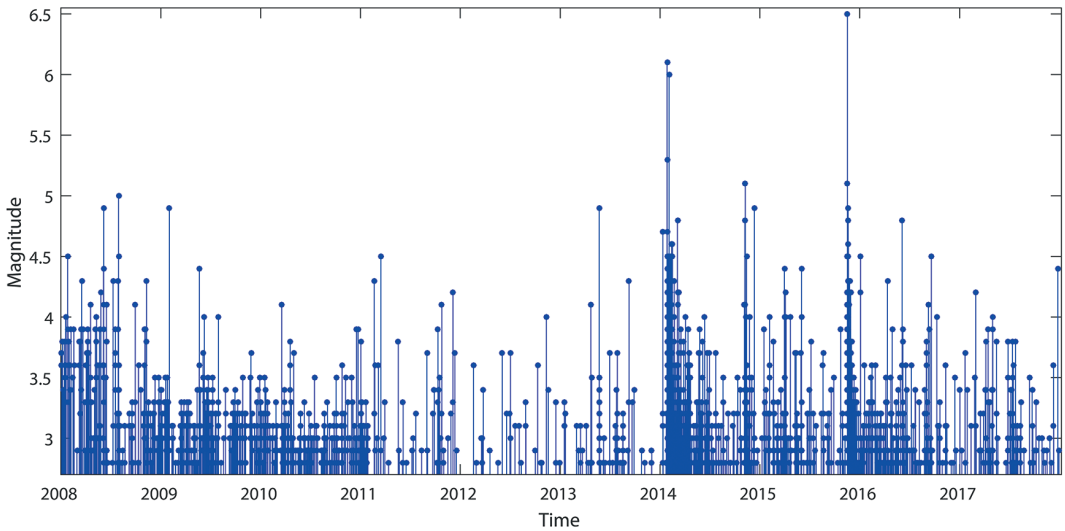

Fig. 4 - Temporal distribution of earthquakes with $M \geq 2.8$ that occurred since 2008.

The M_c is defined as the magnitude at which 95% of the observed data are modelled by a straight line fit, according to the GFT method, which in our case equals to 2.7. The *b* and *a* values, calculated via the maximum likelihood method proposed by Aki (1965), attain values of $b = 0.977 \pm 0.0003$ and $a = 5.142$. The standard deviation estimate for the *b*-value uncertainties is computed with the method introduced by Shi and Bolt (1982). Evaluating the *b*-value of the GR law influences the evaluation of the *a*-value, i.e. the overall seismicity rate, which is very important since they are both crucial for seismic hazard studies (e.g. Wiemer *et al*., 2009). As it will be mentioned in the methodology section, the temporal variations of *b*-values are based on techniques using sliding time windows where either the number of events per window is constant or each window has constant length. In order to avoid biased estimates of *b*-values in some subsets and ensure the completeness of all subsets without depriving much information, we add $\Delta M = 0.1$ and consequently, the magnitude threshold for our computations is set $M_{th} = 2.8$. Although a detailed inquiry of *b*-value variation in moving windows demands for a detailed inquiry of the M_c in each window, a common M_c is more representative for comparison reasons (homogeneous data samples). Particularly in the study area, a common M_c can be considered robust because of the high seismicity rate and the high density of the local seismological network. Thus, the entire data set consists of 2650 events above M_{th} the epicentral distribution of which is shown in the map of Fig. 1 and their temporal distribution in Fig. 4.

3. Methodology

The temporal variation of *b*-values is scrutinised by means of two different techniques calculating consecutive time series of *b*-values. The first is the "constant - time - windows" technique, where fixed length time windows are used, and the second one the "fixed - number - of - events" approach (Tormann *et al*., 2012, 2013; Stallone, 2018). The application and comparison of the results from the aforementioned methods will provide an insight regarding the connection of *b*-value variations and seismicity characteristics.

The first step in the application of the "fixed - number - of - events" method is the identification of the constant number of earthquakes *N* included in each sliding window. When *N* gets larger, i.e. by increasing the window length, the results get smoother and finer variations may not be caught, since a very large *N* could allow the existence of large windows that include both periods of high and low seismicity. If a very small *N* is used instead, computations relate to very small duration, particularly during a seismic sequence. For overcoming the arbitrary selection, the average annual number of events occurred in the selected period with $M \geq M_{th}$ is considered. For validating the results, boundaries within plausible limits of ±50 or ±100 shocks could also be examined (Tormann *et al*., 2013). The *b*-value estimation for each data set of *N* events implies varying lengths of time windows. For example, during a seismic excitation *N* events may occur in just a few days or weeks, whereas during periods of relative quiescence, the time windows may last a few years. Using this technique the same uncertainty across all the time windows is assured (Wiemer *et al*., 1998; Nuannin *et al*., 2005). Since the standard error of the *b*-value depends on the number of events (Aki, 1965), when the sample size is fixed, then the error associated with the estimated *b*-value is constant.

The second technique encompasses fixed length time windows that could range from a few months to several years. When the seismicity rates significantly fluctuate, plausible bias

is expected. Selection of small time windows allows capturing even small, abrupt changes in *b*-values, particularly during a seismic excitation, but when seismicity rate is relatively low, the division of data in small time windows would result in many empty bins. On the other hand, choosing large time windows may fill the empty bins but this could also mean that finer changes in seismicity rate are not tracked and detailed information cannot be extracted.

In both techniques, the length of steps between adjacent windows either of fixed length or of fixed number of events should be defined. The overlap between successive estimates could range from completely un-coincided at all to continuously moving windows. When the overlap is small, the step size and the sensitivity to the selection of the starting point are large. In the overlapping windows, *b*-value estimates and possible variations might be due to the new events entering the window instead of the seismicity over the previous window. Another point that should be clarified when applying the aforementioned techniques is the time at which the *b*-values are plotted, i.e. at the beginning, at the middle, or at the end of the time interval. The most physically accepted choice is to display the *b*-value estimates at the end of the time interval and interpret them in terms of the previous seismicity (Tormann *et al*., 2012, 2013).

In general, temporal *b*-value variations are more difficult to be observed instead of the spatial ones because the temporal ones depend on the differentiation in the network geometry and its detectability (Habermann, 1987; Zuniga and Wiemer, 1999). For that reason, the selection of the proper M_c is crucial (Knopoff *et al*., 1982; Marzocchi *et al*., 2020). To avoid biases in the estimation of *b*-values, it should also be assured that the temporal analysis is constrained to a volume where the seismicity is spatially and temporally homogeneous (Wiemer *et al*., 1998).

4. Results

The two methods mentioned in the previous section are applied using earthquakes with $M \geq 2.8$ that occurred in the study area from 2008 up to 2017. For the "fixed - number - of - events" technique, the average annual number of events is used as the constant length of the moving windows, i.e. $\bar{N}_{ann} = 265$ earthquakes. We show that changing the value of the number of events within reasonable boundaries, e.g. ±50 does not significantly alter the shape of the time series (Fig. 5). When the seismic activity is considerably low, *b*-value estimates are not taken into account, which results to the gap in the curves of the *b*-value time series. The restriction set before estimating *b*-value in a particular window is that the difference between the minimum and the maximum magnitude in each subset should be $\Delta M > 1.5$.

Changing the degree of coincidence from no overlap to 80% induces similar shape of the curves (Fig. 6). In the case of 80% coincidence (green line in Fig. 6), *b*-values continuously increase since the beginning of the study period until October 2011 reaching the value of 1.43, and, then, they gradually decrease. When the 2014 doublet occurs, a significant drop appears, namely from $b = 1.28$ to $b = 0.98$. The lowest *b*-value ($b = 0.84$) is reached in the last days of January 2014, after the first mainshock occurrence and before the second one. The estimations during the seismic sequence are performed in time windows that may last even just 4 days, while when seismicity is relatively low, as shown in Fig. 4, the windows may cover a period longer than 3 years. Then, with some slight fluctuations, an upward trend of *b*-values is observed in the

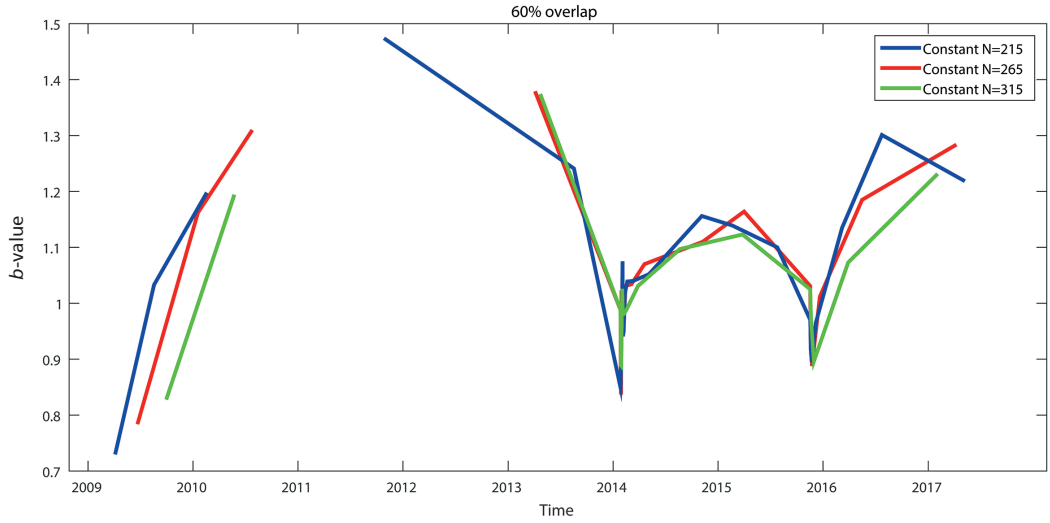

Fig. 5 - Comparison of *b*-value time series using the "fixed - number - of - events" technique versus time: *N* is set 265 events, i.e. the annual average number of events and ±50 events. 60% overlap is set for all cases. The computations refer to the study area depicted in Fig. 1.

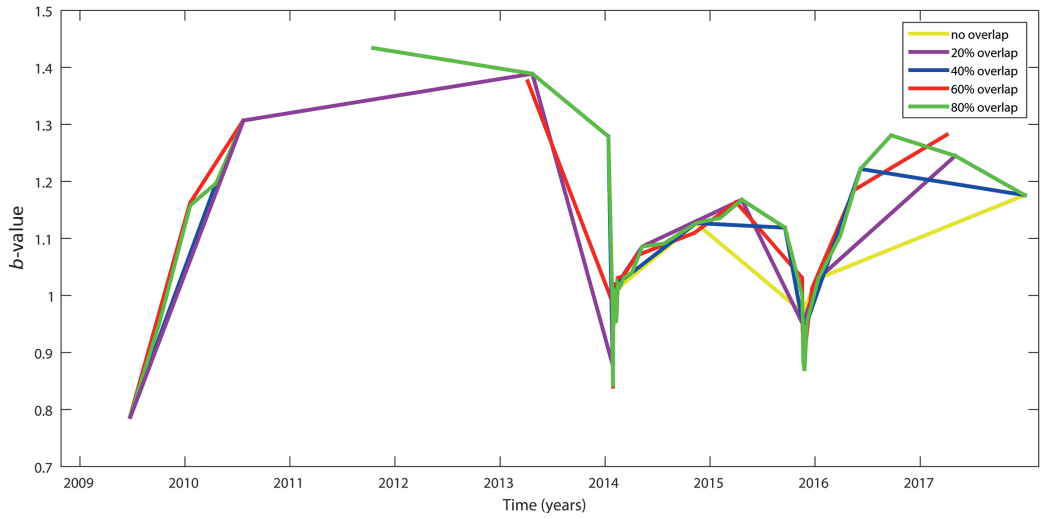

Fig. 6 - Comparison of *b*-value time series using the "fixed - number - of - events" technique versus time with *N* equal to 265 events with different degrees of overlap, from no overlap to 80%. The computations refer to the study area depicted in Fig. 1.

period before the occurrence of the 17 November 2015 M_w 6.5 mainshock. During this aftershock sequence the *b*-values are again decreased up to the $b = 0.87$.

Regarding the "constant - time - windows" technique, a wide range of the time windows duration is examined since both seismic excitation and relative quiescence periods appear in the study period and an average period cannot be considered for the calculations. The duration varies from four months to two years in order to find the most appropriate one with different overlaps. The minimum number of events in each subset should be at least equal to 50 in order to be included in the calculations of *b*-values. The results regarding *b*-value variations are quite

similar with the former approach. Nevertheless, constant moving windows lasting four months do not seem suitable for the interpretation of *b*-value variations due to lack of continuity in the time series attributable to subsets with insufficient data. A constant time window of 2 years seems also inappropriate since this period is comparatively large for detailing the variations. For example, both the January - February 2014 doublet and its aftershock sequence and the November 2015 sequence are included in a constant time window of two years and all the information before and after the mainshocks is lost because a single *b*-value is calculated for the entire period. An intermediate duration of 6 months or 1 year (between 4 months and 2 years) is more suitable as a compromise between gaps and the details regarding *b*-values that appear in a shorter scale.

The yearly seismicity rate is sequentially computed, by setting 80% overlap between successive time windows lasting 1 year and their temporal variation is examined (Fig. 7b), in order to be compared with the corresponding *b*-value variations (Fig. 7a). We observe that, in relative quiescence periods before 2014, the *b*-value raises. On the contrary, when the occurrence rate is increased, which is related to the aftershock sequences of the 2014 Cephalonia doublet and the 2015 Leukas sequence, the *b*-values decrease (Fig. 7a). For every year between 2008 and 2017, the equivalent magnitude per year is calculated, from the cumulatively yearly seismic moment release (Fig. 7c). The decrease in *b*-values corresponds to increase in seismic moment release, particularly in 2014 and 2015, while when seismicity is low between 2011 and 2014, the *b*-values considerably increase.

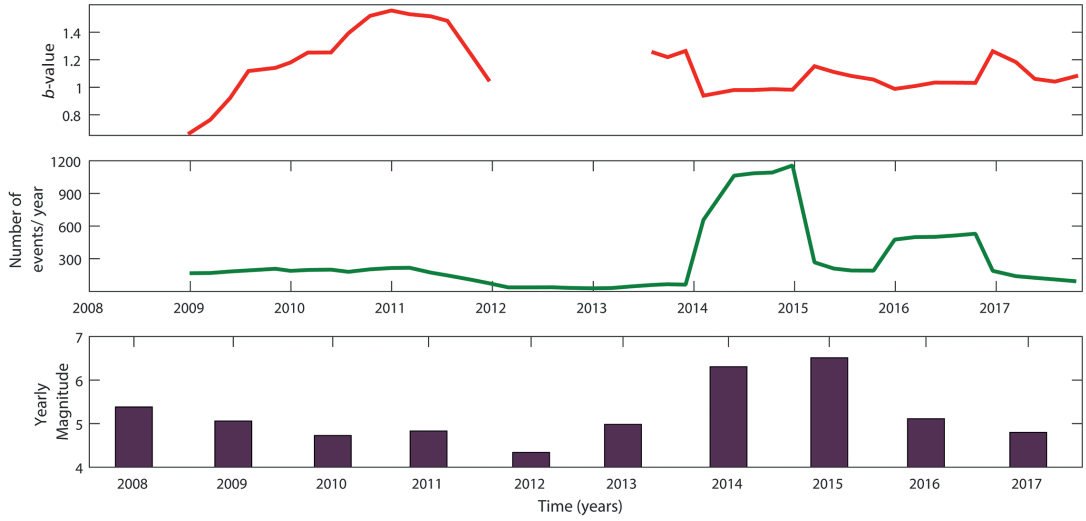

Fig. 7 - a) *b*-value time series using the "constant - time - windows" technique with $T = 1$ year and 80% overlap for the time period from 2008 until 2017; b) rate of events for each consecutive year; c) temporal variations of moment magnitude per year, calculated by summing the annual moment release of earthquakes with $M \geq 2.8$.

For a more extensive investigation, in an attempt to correlate *b*-value fluctuations with the strong earthquakes occurrence, we focused on the last strong sequence of 2015, exploiting the fact that the time after a large mainshock is an exceptionally data rich period (Fig. 8). Particularly, the whole interval between 2008 and 2018 is divided in three sub-periods. The first one corresponds to the long-term background seismicity, covering the period from 2008 until the last event preceding the

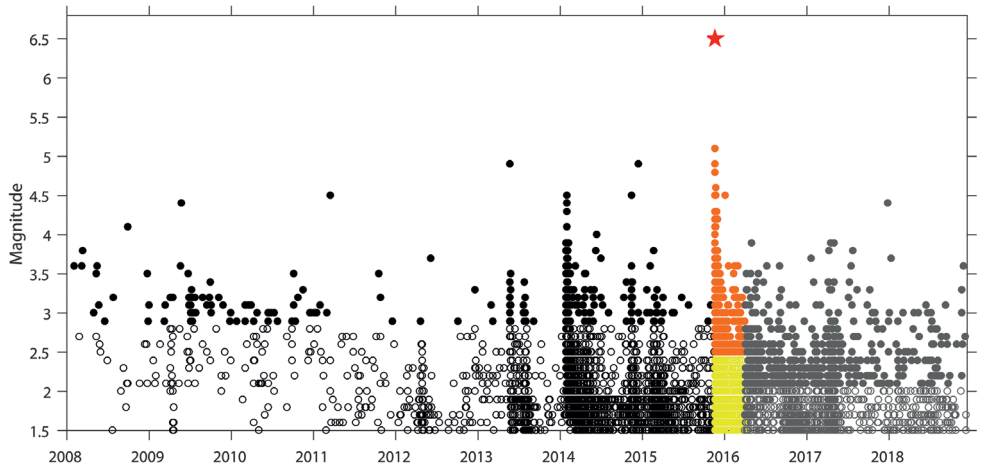

Fig. 8 - Temporal distribution of earthquakes related to the aftershock zone: background (black), during the sequence (orange), after the sequence (grey). Events with magnitude < M_c are depicted with open circles, black, yellow, and grey, respectively. The M_w 6.5 event is depicted with a red star.

2015 M_w 6.5 earthquake. The second sub-period, from 17 November 2015 until 31 March 2016, covers the aftershock sequence and afterwards the next and last one when the activity returned to the background level (Fig. 8). For every sub-period, a different completeness magnitude M_c is considered. The black, orange, and grey circles correspond to the background seismicity, the aftershock activity and the events that occurred in the study area after the occurrence of the sequence, respectively. The open black, yellow, and grey circles are related to the corresponding events with magnitude < M_c that were not taken into account in the current study, i.e. the black circles correspond to the background events with magnitude less than 2.8, the yellow circles are the aftershocks with $M < 2.5$, and the grey circles are events with $M < 2.1$ after the occurrence of the sequence. The M_w 6.5 mainshock is depicted with a red star. For the computations we focus on the area constituting the aftershock zone as defined by Papadimitriou *et al*. (2017), depicted in Fig. 9. In order to examine the *b*-value variations, we choose the "fixed-number-of-events" approach with $N = 50$ events, moving the window over the catalogue stepping by one event and plotting the data at the end of the considered time interval. Selecting such a small window containing only 50 events may be subjected to multiple sources of biases but it is set because of the particularly rich aftershock activity and the fact that small changes could not be captured when a longer window is used.

The magnitude range in each subset, as previously mentioned, should be $\Delta M > 1.5$. Otherwise, a gap is depicted in the curves of the *b*-value time series. At first, we estimate a reference *b*-value for the background seismicity ($b = 1.12$). In general, there is an upward trend until 2012, with *b*-values larger than the reference one, which is reversed when it comes to earthquakes that occurred during 2013. During the sequence of the 2014 doublet, a significant drop is observed with the *b*-values being steadily above 0.76. During 2015, before the occurrence of the mainshock, the *b*-values are rather stabilised around the reference value (Fig. 10a). Immediately after the M_w 6.5 mainshock, significant short term variances are observed, which are lower than the reference value during the first days of the sequence. In a period of approximately one and a half months, *b*-values higher than that of the background seismicity are attained (Fig. 10b). In total, a single *b*-value computed for the sequence is lower than that of the reference *b*-value, $b = 0.95$ (Table 1).

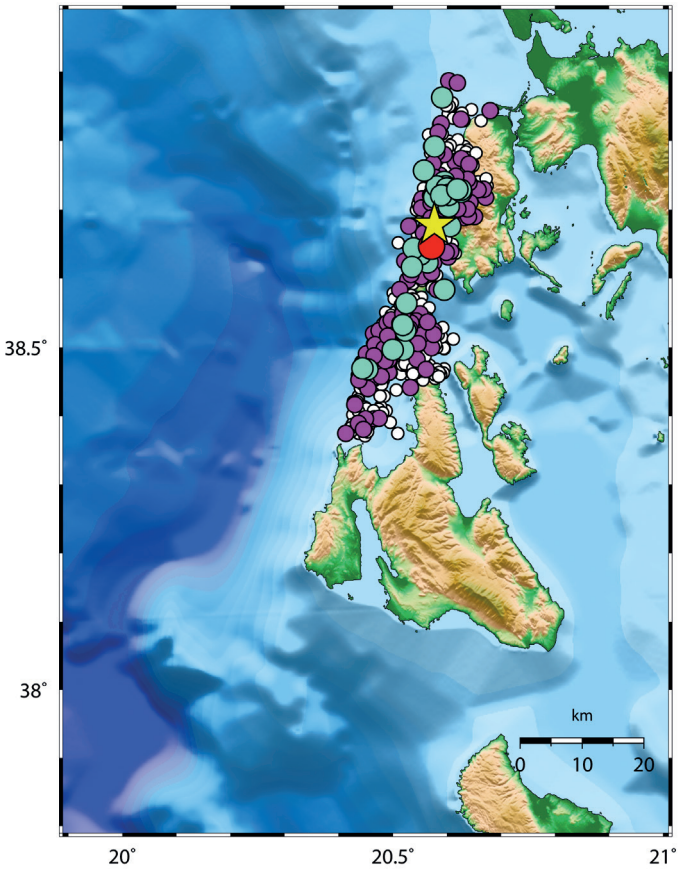

Fig. 9 - Epicentral distribution of earthquakes that occurred between 17 November 2015 and 31 March 2016 in the area around the epicentre of the mainshock. Events with $1.5 \leq M < 3.0$, $3.0 \leq M < 4.0$, $4.0 \leq M < 5.0$, $5.0 \leq M < 6.0$ are depicted with white, magenta, light blue, and red circles, respectively. The M_w 6.5 event is depicted with a yellow star.

Table 1 - Value estimations for the three sub-periods related to the 2015 sequence.

Time interval	Completeness magnitude (M_c)	Number of events	*b*-value estimation
background (01/01/2008 - 17/11/2015)	2.9	310	1.117 ±0.0036
during the sequence (17/11/2015 - 31/03/2016)	2.5	696	0.946 ±0.00014
after the sequence (01/04/2016 - 31/12/2018)	2.1	564	1.008 ±0.0018

After the 2015 sequence the *b*-value increases reaching the reference one ($b = 1.01$). Short term variations are also observed ranging between 0.79 and 1.34 (Fig. 10c).

5. Concluding remarks

Since central Ionian Islands is an area characterised by remarkably high seismic activity, yet with fluctuations in seismicity including also periods of relative quiescence, it is particularly intriguing to investigate the temporal variations of *b*-values and try to correlate them with seismicity variations. Examination of temporal fluctuations of *b*-values is performed by means of

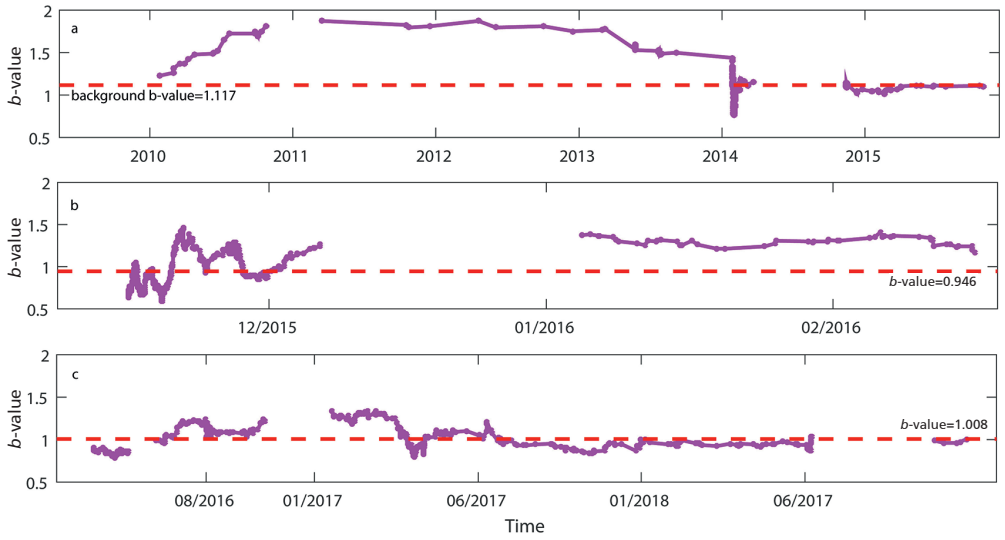

Fig. 10 - Temporal variation of *b*-value throughout the 2015 sequence, related to the aftershock zone depicted in Fig. 9. The red dashed lines represent the *b*-value estimation for the entire subset. The magenta lines are derived by moving the window of $N = 50$ events through the catalogue event by event and plotting the data at the end of the considered time interval. The computations refer to panel: a) the long-term background seismicity, covering the period from 2008 until the last event preceding the M_w6.5 earthquake; b) the period related to the aftershock sequence from 17/11/2015 until 31/03/2016; c) the time interval after the aftershock sequence.

the "fixed - number - of - events" and the "constant - time - windows" approaches. The former is preferred, particularly when dealing with different seismicity rates, due to the same uncertainty observed across all the time windows. The results though are comparable when using windows comprising constant number of earthquakes equal to the average annual number of events or fixed time windows of 6 months or 1 year. In both cases, in periods of intense seismic activity, a decrease in *b*-values is observed, especially during the evolution of the aftershock sequences, whereas when seismicity is low, between 2011 and 2014, an upward trend is noticed. The same conclusion can be deduced when focusing on the aftershock zone of the 2015 Leukas sequence alone. The observed variations suggest that the occurrence of the mainshock is accompanied by a large drop in the *b*-value.

Changes in *b*-value are difficult to establish with confidence, since temporal variation can easily be mimicked or masked by spatial activation changes (Tormann *et al*., 2013). A decrease in *b*-value, when dealing with aftershock sequences, may be due to the larger earthquakes entering the moving window that increase the mean magnitude within the window. It may also be interpreted as an increase in the differential stress on nearby and already tectonically loaded faults that leads to a drop in *b*-value and a subsequent much larger chance of a large event (Gulia and Wiemer, 2019).

Acknowledgements. The constructive comments of two reviewers are acknowledged for their contribution to the improvement of the paper. Gratitude is also extended to M.J. Jimenez for her editorial assistance. The financial support by the European Union and Greece (Partnership Agreement for the Development Framework 2014-2020) under the Regional Operational Programme Ionian Islands 2014-2020, for the project "Telemachus - Innovative Operational Seismic Risk Management System in the Region of Ionian Islands" is gratefully acknowledged. The software Generic Mapping Tools was used to plot the map of the study area (Wessel *et al*., 2013). Geophysics Department Contribution 939.

REFERENCES

Aki K.; 1965: *Maximum likelihood estimate of b in the formula log N = a - bM and its confidence limits*. Bull. Earthquake Res. Inst. Tokyo Univ., **43**, 237-239.

Amitrano D.; 2003: *Brittle-ductile transition and associated seismicity: experimental and numerical studies and relationship with the b value*. J. Geophys. Res.: Solid Earth, **108**, 2044, doi: 10.1029/2001JB000680.

Aristotle University of Thessaloniki Seismological Network; 1981: *Permanent Regional Seismological Network operated by the Aristotle University of Thessaloniki*. International Federation of Digital Seismograph Networks, Other/Seismic Network, Thessaloniki, Greece, doi: 10.7914/SN/HT.

Cao A.M. and Gao S.S.; 2002: *Temporal variations of seismic b-values beneath northeastern Japan island arc*. Geophys. Res. Lett., **29**, 48/1-48/3, doi: 10.1029/2001GL013775.

Ebel J.E., Bonjer K.-P. and Onescu M.V.; 2000: *Paleoseismicity: seismicity evidence for past large eathquakes*. Seismol. Res. Lett., **76**, 283-294.

Goebel T.H.W., Schorlemmer D., Becker T.W., Dresen G. and Sammis C.G.; 2013: *Acoustic emissions document stress changes over many seismic cycles in stick-slip experiments*. Geophys. Res. Lett., **40**, 2049-2054.

Gulia L. and Wiemer S.; 2010: *The influence of tectonic regimes on the earthquake size distribution: a case study for Italy*. Geophys. Res. Lett., **37**, L10305, doi: 10.1029/2010GL043066.

Gulia L. and Wiemer S.; 2019: *Real-time discrimination of earthquake foreshocks and aftershock*. Nature, **574**, 193-199.

Gulia L., Tormann T., Wiemer S., Herrmann M. and Seif S.; 2016: *Short-term probabilistic earthquake risk assessment considering time-dependent b values*. Geophys. Res. Lett., **43**, 1100-1108.

Gulia L., Rinaldi A.P., Tormann T., Vannucci G., Enescu B. and Wiemer S.; 2018: *The effect of a mainshock on the size distribution of the aftershocks*. Geophys. Res. Lett., **45**, 13/277-13/287, doi: 10.1029/2018GL080619.

Gutenberg B. and Richter C.F.; 1944: *Frequency of earthquakes in California*. Bull. Seismol. Soc. Am., **34**, 185-188.

Habermann R.E.; 1987: *Man-made changes of seismicity rates*. Bull. Seismol. Soc. Am., **77**, 141-159.

Hutton K., Woessner J. and Hauksson E.; 2010: *Earthquake monitoring in southern California for seventy-seven years (1932-2008)*. Bull. Seismol. Soc. Am., **100**, 423-446, doi: 10.1785/0120090130.

Kagan Y.Y., Bird P. and Jackson D.D.; 2010: *Earthquake patterns in diverse tectonic zones of the globe*. Pure Appl. Geophys., **167**, 721-741.

Karakostas V., Papadimitriou E., Mesimeri M., Gkarlaouni Ch. and Paradisopoulou P.; 2015: *The 2014 Kephalonia doublet (Mw 6.1 and Mw 6.0) central Ionian Islands, Greece: seismotectonic implications along the Kephalonia transform fault zone*. Acta Geophys., **63**, 1-16, doi: 10.2478/s11600-014-0227-4.

Knopoff L., Kagan Y. and Knopoff R.; 1982: *b values for foreshocks and aftershocks in real and simulated earthquake sequences*. Bull. Seismol. Soc. Am., **72**, 1663-1676.

Marzocchi W., Spassiani I., Stallone A. and Taroni M.; 2020: *How to be fooled searching for significant variations of the b-value*. Geophys. J. Int., **220**, 1845-1856.

Mignan A. and Woessner J.; 2012: *Estimating the magnitude of completeness for earthquake catalogs*. CORSSA (Community Online Resource for Statistical Seismicity Analysis), 45 pp., doi: 10.5078/corssa-00180805.

Naylor M., Orfanogiannaki K. and Harte D.; 2010: *Exploratory data analysis: magnitude, space, and time*. CORSSA (Community Online Resource for Statistical Seismicity Analysis), 42 pp., doi: 10.5078/corssa-92330203.

Nuannin P., Kulhanek O., Persson L. and Askemur T.; 2005: *Inverse correlation between induced seismicity and b-value, observed in the Zingruvan Mine, Sweden*. Acta Geodyn. Geomater., **2**, 5-13.

Papadimitriou E., Karakostas V., Mesimeri M., Chouliaras G. and Kourouklas Ch.; 2017: *The Mw 6.5 17 November 2015 Lefkada (Greece) earthquake: structural interpretation by means of the aftershock analysis*. Pure Appl. Geophys., **174**, 3869-3888.

Papazachos B.C. and Papazachou C.C.; 2003: *The earthquakes of Greece*. Ziti Publication Co., Thessaloniki, Greece, 304 pp.

Papazachos B.C., Kiratzi A.A. and Karakostas B.G.; 1997: *Towards a homogeneous moment-magnitude determination for earthquakes in Greece and the surrounding area*. Bull. Seismol. Soc. Am., **87**, 474-483.

Petruccelli A., Vannucci G., Lolli B. and Gasperini P.; 2018: *Harmonic fluctuation of the slope of the frequency - magnitude distribution (b-value) as a function of the angle of rake*. Bull. Seismol. Soc. Am., **108**, 1864-1876, doi: 10.1785/0120170328.

Petruccelli A., Gasperini P., Tormann T., Schorlemmer D., Rinaldi A.P., Vannucci G. and Wiener S.; 2019: *Simultaneous dependence of the earthquake - size distribution on faulting style and depth*. Geophys. Res. Lett., **46**, 11044-11053, doi: 10.1029/2019GL08399.

Scholz C.H.; 1968: *The frequency-magnitude relation of microfracturing in rock and its relation to earthquakes*. Bull. Seismol. Soc. Am., **58**, 399-415.

Scholz C.H.; 2015: *On the stress dependence of the earthquake b value*. Geophys. Res. Lett., **42**, 1399-1402.

Schorlemmer D. and Wiemer S.; 2005: *Earth science: microseismicity data forecasts rupture area*. Nature, **434**, 1086, doi: 10.1038/4341086a.

Schorlemmer D., Wiemer S. and Wyss M.; 2004: *Earthquake statistics at Parkfield: 1. Stationarity of b-values*. J. Geophys. Res., **109**, B12307, doi: 10.1029/ 2004JB003234.

Schorlemmer D., Wiemer S. and Wyss M.; 2005: *Variations in earthquake size distribution across different stress regimes*. Nature, **437**, 539-542.

Scordilis E.M., Karakaisis G.F., Karakostas B.G., Panagiotopoulos D.G., Comninakis P.E. and Papazachos B.C.; 1985: *Evidence for transform faulting in the Ionian Sea: the Cephalonia Island earthquake sequence of 1983*. Pure Appl. Geophys., **123**, 388-397, doi: 10.1007/BF0080738.

Shi Y. and Bolt B.A.; 1982: *The standard error of the magnitude-frequency b value*. Bull. Seismol. Soc. Am., **72**, 1677-1687.

Stallone A.; 2018: *Statistical analysis of earthquake occurrences and implications for earthquake forecasting and seismic hazard assessment*. Ph.D. Thesis, University of Roma Tre, doi: 10.13140/RG.2.2.35672.65282/1.

Stein R.S.; 1999: *The role of stress transfer in earthquake occurrence*. Nature, **402**, 605-609, doi: 10.1038/45144.

Tormann T., Wiemer S. and Hauksson E.; 2010: *Changes of reporting rates in the Southern Californian Earthquake Catalog, introduced by a new definition of ML*. Bull. Seismol. Soc. Am., **100**, 1733-1742.

Tormann T., Wiemer S. and Hardebeck J.; 2012: *Earthquake recurrence models fail when earthquakes fail to reset the stress field*. Geophys. Res. Lett., **39**, L18310, doi: 10.1029/2012GL052913.

Tormann T., Wiemer S., Metzger S., Michael A. and Hardebeck J.; 2013: *Size distribution of Parkfield's microearthquakes reflects changes in surface creep rate*. Geophys. J. Int., **193**, 1474-1478, doi: 10.1093/gji/ggt093.

Tormann T., Wiemer S. and Mignan A.; 2014: *Systematic survey of high-resolution b value imaging along Californian faults: inference on asperities*. J. Geophys. Res., **119**, 1-26.

Tormann T., Enescu B., Woessner J. and Wiemer S.; 2015: *Randomness of megathrust earthquakes implied by rapid stress recovery after the Japan earthquake*. Nat. Geosci., **8**, 152-158, doi: 10.1038/ngeo2343.

Utsu T.; 1999: *Representation and analysis of the earthquake size distribution: a historical review and some new approaches*. Pure Appl. Geophys., **155**, 509-535.

Wiemer S. and Wyss M.; 1997: *Mapping the frequency-magnitude distribution in asperities: an improved technique to calculate recurrence times?* J. Geophys. Res., **102**, 15115-15128.

Wiemer S. and Wyss M.; 2000: *Minimum magnitude of complete reporting in earthquake catalogs: examples from Alaska, the western United States, and Japan*. Bull. Seismol. Soc. Am., **90**, 859-869, doi: 10.1785/0119990114.

Wiemer S. and Wyss M.; 2002: *Mapping spatial variability of the frequency-magnitude distribution of earthquakes*. Adv. Geophys., **45**, 259-302.

Wiemer S., McNutt S. and Wyss M.; 1998: *Temporal and three-dimensional spatial analyses of the frequency-magnitude distribution near Long Valley Caldera, California*. Geophys. J. Int., **134**, 409-421.

Wiemer S., Giardini D., Faeh D., Deichmann N. and Sellami S.; 2009: *Probabilistic seismic hazard assessment of Switzerland: best estimates and uncertainties*. J. Seismol., **13**, 449-478, doi: 10.1007/s10950-008-9138-7.

Woessner J. and Wiemer S.; 2005: *Assessing the quality of earthquake catalogues: estimating the magnitude of completeness and its uncertainty*. Bull. Seismol. Soc. Am., **95**, 684-698, doi: 10.1785/0120040007.

Wyss M. and Wiemer S.; 2000: *Change in the probabilities for earthquakes in southern California due to the Landers M 7.3 earthquake*. Sci., **290**, 1334-1338.

Wyss M., Nagamine K., Klein F.W. and Wiemer S.; 2001: *Evidence for magma at intermediate crustal depth below Kilauea's East Rift, Hawaii, based on anomalously high b-values*. J. Volcanol. Geotherm. Res., **106**, 23-37.

Zuniga F.R. and Wyss M.; 1995: *Inadvertent changes in magnitude reported in earthquake catalogs: influence on b-value estimates*. Bull. Seismol. Soc. Am., **85**, 1858-1866.

Zuniga F.R. and Wiemer S.; 1999: *Seismicity patterns: are they always related to natural causes?* Pure Appl. Geophys., **155**, 713-726.

Zuniga F.R., Suárez G., Figueroa-Soto Á. and Mendosa A.; 2017: *A first-order seismotectonic regionalization of Mexico for seismic hazard and risk estimation*. J. Seismol., **21**, 1295, doi: 10.1007/s10950-017-9666-0.

Corresponding author: Ourania Mangira
Department of Geophysics, School of Geology, Aristotle University of Thessaloniki
University Campus, GR54124 Thessaloniki, Greece
Phone: +30 2310 998536; e-mail: omangira@geo.auth.gr